

Plasmon–Polaron Coupling in Conjugated Polymer on Infrared Nanoantennas

Wang, Zilong; Zhao, Jun; Frank, Bettina; Ran, Qiandong; Adamo, Giorgio; Giessen, Harald; Soci, Cesare

2015

Wang, Z., Zhao, J., Frank, B., Ran, Q., Adamo, G., Giessen, H., et al. (2015). Plasmon–polaron coupling in conjugated polymer on infrared nanoantennas. *Nano Letters*, 15(8), 5382-5387.

<https://hdl.handle.net/10356/82772>

<https://doi.org/10.1021/acs.nanolett.5b01760>

© 2015 American Chemical Society. This is the author created version of a work that has been peer reviewed and accepted for publication by *Nano Letters*, American Chemical Society. It incorporates referee's comments but changes resulting from the publishing process, such as copyediting, structural formatting, may not be reflected in this document. The published version is available at: [<http://dx.doi.org/10.1021/acs.nanolett.5b01760>].

Downloaded on 20 Mar 2024 17:35:22 SGT

Plasmon–Polaron Coupling in Conjugated Polymer on Infrared Nanoantennas

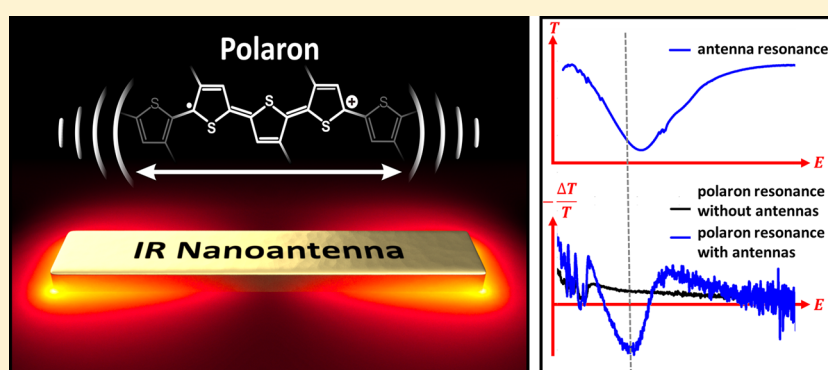
Zilong Wang,^{†,‡} Jun Zhao,[§] Bettina Frank,[§] Qiangdong Ran,[†] Giorgio Adamo,[‡] Harald Giessen,^{‡,§} and Cesare Soci^{*,†,‡}

[†]Division of Physics and Applied Physics, School of Physical and Mathematical Sciences, Nanyang Technological University, Singapore 637371

[‡]Centre for Disruptive Photonic Technologies, Nanyang Technological University, Singapore 637371

[§]4th Physics Institute and Research Center SCoPE, University of Stuttgart, Pfaffenwaldring 57, 70569 Stuttgart, Germany

S Supporting Information



ABSTRACT: We propose and demonstrate a novel type of coupling between polarons in a conjugated polymer and localized surface plasmons in infrared (IR) nanoantennas. The near-field interaction between plasmons and polarons is revealed by polarized photoinduced absorption measurements, probing mid-IR polaron transitions, and infrared-active vibrational modes of the polymer, which directly gauge the density of photogenerated charge carriers. This work proves the possibility of tuning the polaronic properties of organic semiconductors with plasmonic nanostructures.

KEYWORDS: Localized surface plasmons, IR nanoantennas, conjugated polymer, polarons

The coupling of plasmons to various degrees of freedom, such as molecular vibrations,^{1,2} phonons,^{3,4} and excitons^{5–7} in hybrid nanostructured materials is a subject of intense investigation. Local electric field enhancement in the vicinity of plasmonic nanostructures is regarded as an effective light-trapping technique^{8,9} and also as a method to modify the photophysical properties of materials.^{10,11} In the area of organic semiconductors, applications of plasmonic nanostructures range from the enhancement of light emission and collection efficiency in light-emitting devices¹² to the improvement of light harvesting in thin-film photovoltaics.^{13,14} Specifically, coupling of triplet states in polymers with near-IR plasmon resonances of silica core–gold shell nanoparticles allowed inducing quenching of radiative triplet exciton recombination and reducing polymer susceptibility to photo-oxidative degradation.⁶ In thin film polymer photovoltaics, plasmonic electric-field enhancement is often used to increase light absorption by coupling surface plasmon resonances with excitonic transitions of the polymer, at energies above the highest occupied molecular orbital (HOMO) and the lowest unoccupied molecular orbital (LUMO) gap.¹⁵ Increased probability of exciton dissociation via plasmon–exciton

coupling has also been reported.^{16–18} While neutral exciton species are responsible for light absorption and emission properties organic materials, self-localized polarons induced by strong electron–phonon coupling fully determine their charge transport characteristics.^{19,20} Unlike previous studies on plasmon hybridization with excitons in organic semiconductors, here we focus on the interaction between surface plasmons and photogenerated polarons in a conjugated polymer. By engineering a plasmonic metamaterial resonant with characteristic infrared polaronic transitions, we provide evidence, for the first time, of plasmon–polaron coupling as a means to modify charged photoexcitations of organic materials.

The proposed concept is illustrated in Figure 1a. Photo-generated polarons along the polymer backbones interact with localized surface plasmons in the adjacent IR nanoantennas, which resonate at characteristic mid-IR polaron energies far from excitonic absorption. Plasmon–polaron coupling is

Received: May 5, 2015

Revised: July 4, 2015

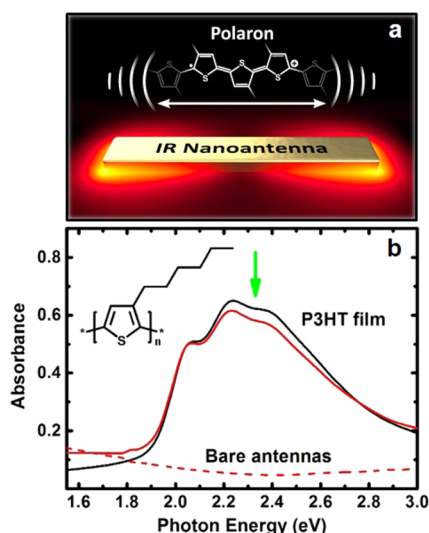


Figure 1. Schematic representation of plasmon–polaron coupling and absorption spectra of P3HT and nanoantennas. (a) Localized surface plasmons excited by the external IR light field (the red cloud depicts the localized field distribution of the nanoantennas) interact with positive polarons (radical cations) generated by visible light excitation on the polymer chains. (b) Absorption spectra of pristine P3HT film (black solid curve), IR-nanoantennas/P3HT hybrid sample (red solid curve) and bare IR-antennas (red dash curve). The green arrow indicates the excitation photon energy used in experiments. Inset is the molecular structure of P3HT.

55 expected to resonantly enhance oscillator strength of polaronic
56 transitions and to possibly alter the polaron relaxation and
57 exciton dissociation dynamics.²¹ To test this concept we chose
58 the well-characterized organic photovoltaic material regiore-

gular poly(3-hexylthiophene) (rr-P3HT),^{22,23} whose chemical
structure shown in Figure 1b P3HT is a low-bandgap polymer
(HOMO–LUMO gap ~ 1.9 eV) with absorption spectrum
(solid black curve in Figure 1b) well overlapped with solar
irradiance. As first suggested by the Su–Schrieffer–Heeger
(SSH) tight-binding model,¹⁹ the generation of polarons in
conjugated polymers results in the formation of new intragap
states associated with positive and negative polaron relaxation
energies (Figure 2a). In P3HT, such intragap states lead to the
appearance of two infrared optical transitions (P_1 and P_2 in the
left diagram in Figure 2a); the corresponding photoinduced
absorption (PIA) spectrum in Figure 2b shows P_1 and P_2
polaron absorption bands around 0.33 and 1.24 eV,
respectively. In addition to polaron transitions, characteristic
infrared active vibrational (IRAV) modes due to the presence of
charged species on the polymer chain are evident at the low-
energy side of the PIA spectrum, below 0.16 eV.²³ The intensity
of polaron transitions and IRAV modes can be used as a unique
gauge for charge carrier density in conjugated polymers.^{24,25}

To induce coupling between plasmon and polarons, we
designed and fabricated metal nanostructures with resonant
features overlapped with the P_1 polaron band and negligible
absorption in the visible part of the spectrum to avoid
plasmonic enhancement of excitonic absorption. For similar
reasons, we avoided coupling with P_2 because of its overlap
with the broadband excited state absorption of interchain
excitons (EX) at 1.05 eV.^{26,27} The structure of choice was a
split-ring resonator (SRR) with geometrical parameters shown
in Figure 2c. The corresponding transmission spectra obtained
by numerical simulations for orthogonal polarizations of the
incident light are shown in Figure 2d (polarization directions
with respect to SRR gap orientation are depicted as a blue
arrow for 90° and a red arrow for 0° in Figure 2c). A single

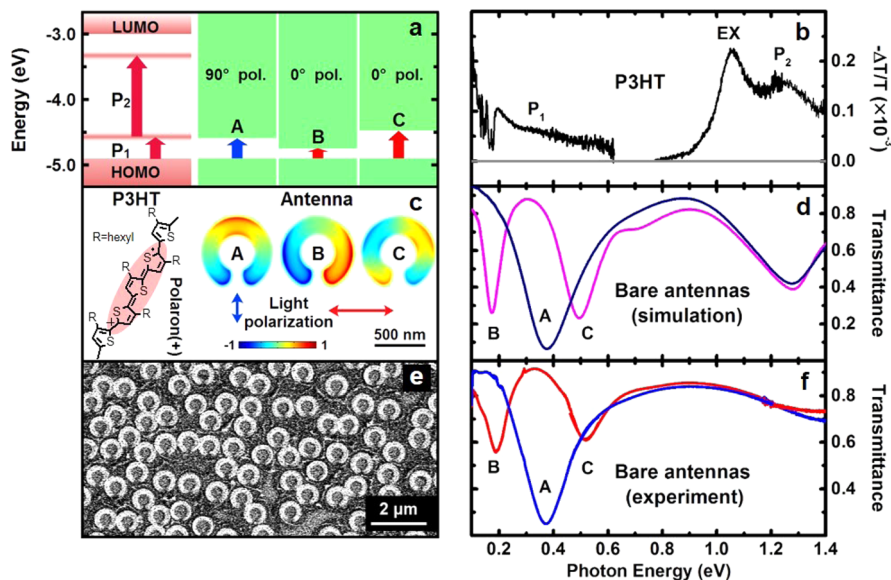


Figure 2. Characterization of P3HT and large area IR-nanoantennas. (a) Molecular orbital energy diagram of polaron transitions in P3HT (left, pink), and resonance transitions of IR-nanoantennas with 0° and 90° polarized light excitation (right, green). (b) P3HT polaron bands in PIA spectra: the P_1 and P_2 bands correspond to polaronic transitions, the EX peak originates from interchain singlet excitons. (c) Schematic representation of a localized positive polaron on the P3HT chain (left) and simulated near field maps of E_z above the split ring resonator (right); dipolar modes appear at A and B, the quadrupolar mode at C. The blue and red arrows indicate the direction of incident light polarization. (d) Simulated transmission spectra of bare antennas for 0° (violet curve) and 90° (navy blue curve) polarized light; A, B, and C correspond to resonant modes in panel c. (e) SEM image of fabricated large area nanoantennas with SRR structures. (f) Measured transmission spectra of bare nanoantennas for orthogonal polarizations (0° , red curve and 90° , blue curve).

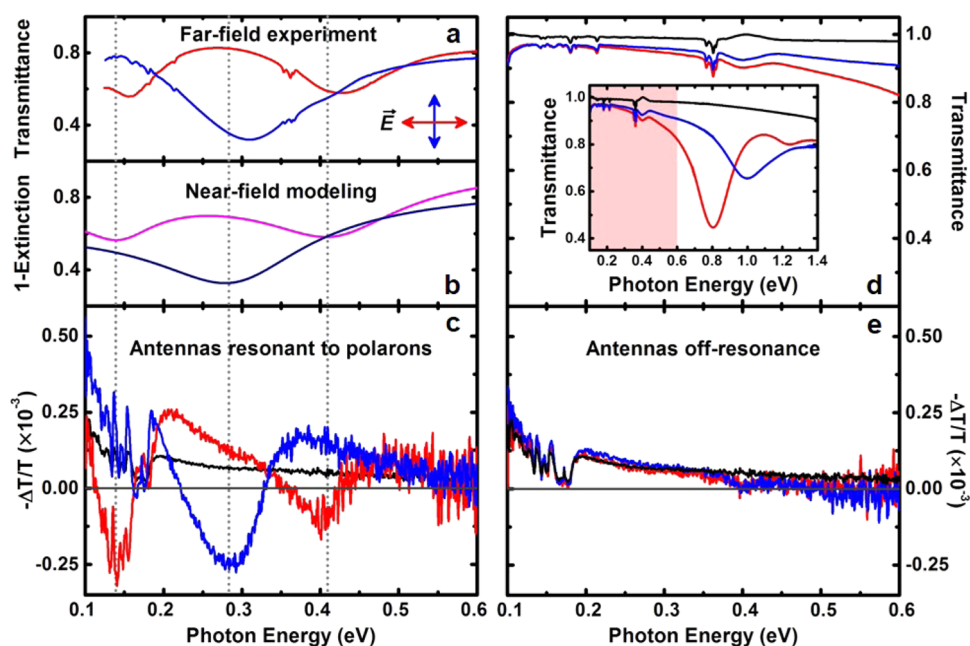


Figure 3. PIA spectra of P3HT on nanoantennas in the mid-IR region. (a) Measured transmission spectra of P3HT film on IR-nanoantennas for 0° (red curve) and 90° (blue curve) light polarization. (b) Calculated near-field resonances of the SRRs using a damped harmonic oscillator model (violet curve for 0° and navy blue curve for 90° polarized light). (c) PIA spectra of pristine P3HT (black curve) IR-nanoantennas/P3HT hybrid sample for 0° (red curve) and 90° (blue curve) polarized probe light; vertical dashed lines are guideline to highlight the resonance shift from the far- to the near-field of the SRRs. (d) MIR transmission spectra of pristine P3HT thin film on CaF₂ (black curve) and hybrid polymer on off-resonance nanoantennas (control sample) for 0° (red curve) and 90° (blue curve) light polarizations. Inset: transmission spectra extended to the near-infrared region show resonance positions of the control sample (the pink region corresponds to the enlarged axes of the main panel). (e) PIA spectra of P3HT on control sample (red curve for 0° and blue curve for 90° polarized probe light) and pristine P3HT thin film on CaF₂ as a reference (black curve).

92 resonance around 0.37 eV (A in Figure 2d) is excited in the
93 region of interest for 90° polarization, while two resonances
94 appear in the same region, at 0.19 eV (B) and 0.53 eV (C) for
95 0° polarization of the incident wave. The energy diagrams of
96 these three transitions are shown alongside the P3HT polaronic
97 transitions in Figure 2a; when taking into account the red-shift
98 induced on plasmonic resonance frequency by the high-index
99 polymer film, the A and B plasmonic resonances are optimally
100 aligned with the P₁ transition and the IRAV modes of P3HT.
101 Normalized field distributions of the electric field component
102 perpendicular to the plane of the structure (E_z) 20 nm above
103 the substrate plane for each SRR resonance are plotted in
104 Figure 2c and show near-field confinement of the fields due to
105 surface plasmon resonant modes in the SRR. Clear dipolar
106 modes can be identified for A and B, while a quadrupolar mode
107 is excited at higher frequency (C) as expected.

108 On the basis of this design, large-area SRR samples were
109 fabricated using hole-mask colloidal nanolithography with
110 tilted-angle-rotation evaporation, a proven technique for low-
111 cost and large-area fabrication of complex plasmonic nano-
112 structures and metamaterials (see Supporting Information for
113 sample fabrication methods).^{28,29} Resulting samples comprise a
114 dense array of SSRs, where the metamolecules are randomly
115 distributed but share a common rotational orientation
116 throughout the entire substrate (see electron microscope
117 image in Figure 2e). Consequently, large-area transmission
118 spectra of fabricated structures for 0° and 90° light polarization
119 (Figure 2f) agree very well with simulations obtained with
120 periodic boundary conditions (Figure 2d). Following the design
121 requirements, the fabricated IR-nanoantennas have very low
122 absorbance (OD < 0.1) in the visible part of the spectrum

overlapped with absorption of P3HT (red dashed curve in
Figure 1b). Absence of plasmonic enhancement of polymer
absorption is confirmed by the slight quenching of P3HT film
absorption (black solid curve in Figure 1b) on the IR-
nanoantennas (red solid curve in Figure 1b). This ensures that
visible excitation (e.g., at 532 nm, green arrow in Figure 1b) of
the hybrid metamaterial/polymer sample photoexcites the
polymer but not the IR-nanoantennas. The topography of the
IR-nanoantennas/P3HT sample shows a homogeneous cover-
age of polymer film with thickness of 70 nm (Figures S1 and S2
in Supporting Information).

Polarized infrared transmission of the hybrid film is shown in
Figure 3a. Both spectra obtained with 0° and 90° polarizations
(red and blue curves) present characteristic features of P3HT
(e.g., the hexyl C–H stretching vibrational modes at ~0.36 eV)
as well as of the nanoantennas (e.g., polarized resonances). The
high refractive index ($n \sim 1.85$) of the polymer film induces a
red shift of about 0.06 eV of the nanoantenna resonances with
respect to the bare antennas (Figure 2f). Moreover, interaction
between the surface plasmons of the SRR and the polarons in
the polymer occurs in the near-field of the nanostructures,³⁰
whereby near-field resonances are typically red shifted when
compared to the far-field response. This near-field shift is well
described by a damped harmonic oscillator model driven by an
external light field.^{31,32} Figure 3b shows the simulated near-field
spectra of our SRRs corresponding to the fitting parameters of
Lorentz oscillators extracted from the transmission spectra in
Figure 3a, where near-field resonances are further red shifted by
~0.11 eV compared to the far field ones.

To probe the interaction between resonant surface plasmons
and polarons in the hybrid metamaterial/P3HT system we

conducted broadband steady-state PIA experiments at low temperature, $T = 78$ K, using visible laser excitation as the “pump” and the polarized broadband beam of a Fourier-transform infrared spectrometer as the “probe”; the corresponding differential transmittance spectra are reported in Figure 3c (see measurement descriptions in Supporting Information). The PIA of the hybrid metamaterial/P3HT sample is found to be independent of pump beam polarization but strongly dependent on the polarization of the probe. As anticipated, the resonant enhancement of PIA spectra coincides with the near-field resonances calculated in Figure 3b, which can be regarded as strong evidence of plasmon–polaron coupling. Moreover, for both 0° (red solid curve) and 90° (blue solid curve) polarizations the amplitude of PIA resonances is enhanced by a factor of approximately two compared to the reference pristine P3HT film (black solid curve), indicative of plasmon-induced enhancement of the polaron density. The actual enhancement factor of the PIA signal is masked by the strong modulation features appearing at 0.14 and 0.41 eV for the 0° polarization and at 0.29 eV for the 90° polarization, which make a quantitative analysis difficult. To further understand these modulation features, we subtracted the PIA signal of IR-nanoantennas/P3HT from that of pristine P3HT. The resulting spectrum shows photobleaching of P3HT polaron absorption induced by the IR-nanoantennas, which may be attributed to the resonant transfer of charges into corresponding P3HT polaron states upon the excitation of IR-nanoantennas (Figure S3 and discussions in Supporting Information). To rule out other factors such as charge or energy transfer from the polymer to the nanoantennas,³³ or improved morphology of polymer films spun-cast on metals on the polaron signal enhancement,³⁴ we fabricated a control sample with plasmonic nanoantennas off-resonance with respect to polarons mid-infrared (MIR) transitions (Figure S3d) and characterized it under the same experimental conditions (the characterization of the off-resonance sample is shown in Figure S4 in Supporting Information). In this case, probe-polarized PIA spectra of the control sample show very similar behavior to that of pristine P3HT films with no significant enhancement of the polaron signal (Figure 3e).

The effect of plasmon–polaron coupling is also reflected by changes of vibrational absorption spectra of P3HT upon photodoping. Various theoretical studies describe the appearance of strong IRAV modes when even parity symmetric Raman-active vibrational modes (A_g modes) are converted into IR-active modes by the local symmetry breaking of polymer chains produced by charge localization.^{24,35,36} Experimental infrared absorption spectra induced by photo- or chemical-doping show peaks with one-to-one correspondence to the strongest Raman-active modes of the polymer observed in resonance Raman scattering.³⁷ The intensity of these IRAV modes is directly proportional to charge carrier concentration, making them a unique optical probe for charge carrier density and dynamics in conjugated polymers.^{25,38} Instead of manifesting as PIA peaks, IRAV modes of P3HT films possess a Fano-type antiresonance line shape (Figure 4b), created by the superposition of the narrow IRAV modes with the broadband delocalized polaron absorption.^{27,39} In Figure 4b, we compare the IRAV modes of the pristine polymer film (black curve) with those obtained from the hybrid IR-nanoantennas/P3HT sample with orthogonal probe polarizations. For 90° polarization (blue curve), the IRAV modes appear in a spectral region not strongly modulated by the

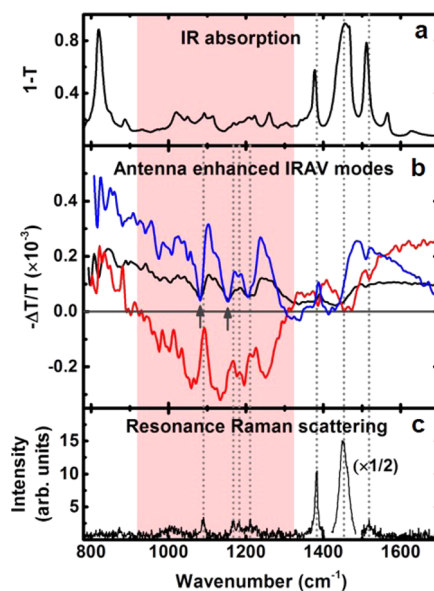


Figure 4. IRAV modes in P3HT on nanoantennas. (a) IR absorption spectrum of P3HT. (b) IRAV modes below 1700 cm^{-1} in PIA spectra for pristine P3HT film (black solid curve) and IR-nanoantennas/P3HT hybrid film at 0° (red solid curve) and 90° (blue solid curve). Dashed gray line arrows indicate IR and Raman active modes; solid gray arrow indicate typical IRAV antiresonances in 90° polarized PIA spectra that become clear peaks for 0° polarization. Pink area indicates the typical IRAV modes area in spectrum. (c) Resonance Raman scattering spectrum of P3HT thin film.

plasmon–polaron coupling resonance at ~ 0.3 eV; nevertheless, their intensity is enhanced by more than a factor of 2 and all modes are preserved without spectral shift with respect to the pristine film. In both pristine and hybrid samples at 90° probe polarization (black and blue curves in Figure 4b), the assignment of IRAV modes to P3HT IR-absorption (Figure 4a) and resonance Raman (Figure 4c) modes is hindered by the presence of antiresonances (indicated by gray arrows). In contrast, at 0° probe polarization the IRAV modes overlap with the plasmon–polaron coupling resonance at ~ 0.15 eV, and their peaks are easily resolved (red curve in Figure 4b): from 900 to 1300 cm^{-1} , the antiresonances become positive IRAV peaks perfectly matching the Raman active modes, whereas in the tail of the modulation from 1300 to 1700 cm^{-1} the IRAV peaks become antiresonances, also in correspondence with Raman active modes. We therefore speculate that the near-field coupling of plasmons and polarons offsets the effect of broadband delocalized polaron absorption in the spectra, thus making IRAV modes of P3HT clearly distinguishable; these experimental results are consistent with the description from nonadiabatic amplitude mode theory developed by Horovitz and colleagues.³⁹ The enhancement of IRAV modes in both 0° and 90° polarized PIA spectra may suggest that more charges are generated in IR-nanoantennas/P3HT hybrid sample.

To further elucidate the plasmon–polaron coupling mechanism and its effect on inherent photophysical properties of the polymer, such as polaron generation, we compare infrared PIA spectra to differential transmittance spectra obtained upon chemical (redox) doping^{37,40} of pristine P3HT and P3HT on resonant nanoantennas (Figure 5). By chemically introducing charge carriers, we rule out the possibility that the enhancement observed in PIA spectra may arise from additive effects of plasmonic and polaronic absorption resonances and

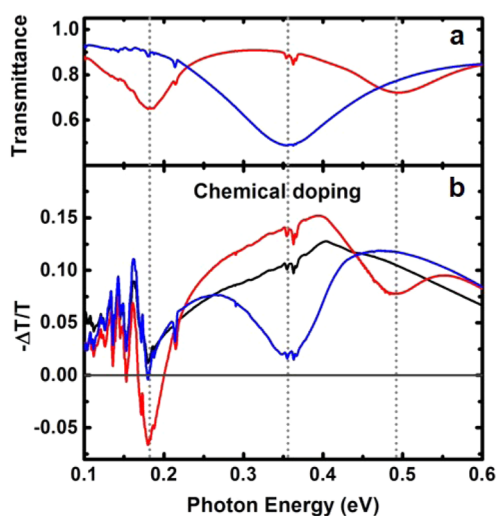


Figure 5. Chemical doping-induced absorption spectra of P3HT on nanoantennas. (a) Transmission spectra of undoped IR-nanoantennas/P3HT hybrid sample with 0° (red curve) and 90° (blue curve) light polarizations. (b) Chemical doping induced absorption spectra for pristine P3HT film (black curve) and hybrid sample at 0° (red curve) and 90° (blue curve) polarizations. Dashed lines indicate the spectral position of far-field transmission resonances. $-\Delta T/T$ here indicates relative change of transmission spectra of the sample as in Figure 3a–c upon chemical doping.

thermal, photon energy, or electric field activation.^{41–43} Experiments clearly demonstrate that both exciton and polaron photogeneration are ultrafast ($t < 100$ fs) events^{25,44} with polaron/exciton branching ratios varying from 10% to 30% in pristine polymer films.^{45,46} There are two possible mechanisms by which plasmon–polaron coupling with IR nanoantennas could lead to enhanced polaron photogeneration yield: (i) formation of plasmon–polaron complexes may favor direct polaron relaxation through resonant energy transfer; (ii) absorption of IR light by the coupled resonant nanoantennas may provide excess thermal energy needed for exciton dissociation.⁴⁷ Additional studies will be required to elucidate these arguments, such as “pump-push-probe” experiments^{48,49} or measurements of photocurrent generation in working device structures.

In conclusion, we have demonstrated, via photoinduced absorption spectroscopy, a new plasmon–polaron coupling mechanism in P3HT polymer films by engineering the plasmonic nanoantennas resonance to overlap in energy with the P3HT polaron absorption. These findings could potentially open new routes toward the design of more efficient organic photodetector and photovoltaic devices through carefully engineered metamaterials that recycle the infrared solar radiation to promote direct carrier photogeneration and exciton dissociation in polymers and donor–acceptor bulk heterojunctions.^{49,50} It may also be possible to engineer plasmonic nanostructures with resonances in the vis-NIR spectral region to enhance photon absorption and in the mid-IR to enhance polaron photogeneration simultaneously. Moreover, plasmon–polaron coupling demonstrated here may have further implications in functional materials other than conjugated polymers and broadly in nanophotonics. In solid-state systems, one could envision plasmonic tuning of the photogenerated polaron and bipolaron density or of photoinduced local modes of superconducting cuprates;⁵¹ in plasmonic systems, one could exploit polarons in organic semiconductors to achieve strong coupling with metamaterials⁵² or to design dispersion relation of propagating hybrid surface-polaron–plasmon polaritons.

■ ASSOCIATED CONTENT

§ Supporting Information

Experimental descriptions, IR nanoantennas fabrication methods, AFM images, more discussions of modulation features, and characterization of off-resonance sample are included. The Supporting Information is available free of charge on the ACS Publications website at DOI: 10.1021/acs.nanolett.5b01760.

■ AUTHOR INFORMATION

Corresponding Author

*E-mail: csoci@ntu.edu.sg.

Notes

The authors declare no competing financial interest.

■ ACKNOWLEDGMENTS

C.S. thanks Professor Guglielmo Lanzani for fruitful discussions at the conception stage of this work. The authors are grateful to Paola Lova for assistance with chemical doping and to Nikolai Strohhfeldt for realizing some of the graphics. Research was supported by the Singapore Ministry of Education (Grants MOE2011-T3-1-005 and MOE2013-T2-1-044) and Nanyang Technological University (NAP startup Grant M4080511). The Stuttgart group acknowledges funding by DFG, BMBF, 344

conclude instead that the near-field coupling between the quasi-particles induces an actual change of the polymer excited state. Even in this case, both plasmonic resonances and polymer absorption features are clearly visible in MIR far-field transmission spectra of the hybrid nanoantennas/P3HT film (Figure 5a). Doping-induced absorption spectra of pristine P3HT (black curve) and hybrid nanoantennas/P3HT probed with 0° and 90° polarized light (red and blue curves, respectively) in Figure 5b exhibit the following features: (i) broad polaron absorption, centered around 0.4 eV, similar to PIA spectra of pristine P3HT (see Figure 2b), and polarized modulations induced by resonant plasmon coupling in the hybrid sample (red and blue curves); (ii) no significant enhancement or spectral shift of the resonances induced by near-field coupling, for either of the polarizations; (iii) no enhancement of IRAV mode intensity (below 0.18 eV) in the hybrid film compared to the pristine P3HT film on either probe polarization. Features (ii) and (iii) indicate that no polarons are generated due to the coupling to surface plasmons in addition to those that are chemically induced. Therefore, we argue that the mechanism leading to enhanced polaron transitions in the presence of resonant IR nanoantennas must be dynamic and may be due to the thermal activation of polaron photoexcitation (which does not occur in the case of static, chemical doping), rather than to a purely spectroscopic effect. We emphasize that the PIA experiments involve a three-level system comprising the main excitonic transition of the polymer in resonance with the pump, as well as photoinduced polaronic transitions and nanoantenna plasmonic modes in resonance with the infrared probe; it appears that both infrared resonances must be excited simultaneously to lead to cooperative enhancement of polaronic transitions.

The generally accepted scheme for polaron photogeneration in conjugated polymers sees a competing pathway between direct photoexcitation and exciton dissociation. While the first process does not require any excess energy, the second requires

345 Alexander-von-Humboldt-Stiftung, BW-Stiftung, Zeiss-Stiftung,
346 and EU through the ERC Advanced Grant COMPLEXPLAS.

347 ■ REFERENCES

- 348 (1) Neubrech, F.; Pucci, A.; Cornelius, T. W.; Karim, S.; García-
349 Etxarri, A.; Aizpurua, J. *Phys. Rev. Lett.* **2008**, *101*, 157403.
- 350 (2) Dregely, D.; Neubrech, F.; Duan, H.; Vogelgesang, R.; Giessen,
351 H. *Nat. Commun.* **2013**, *4*, 2237.
- 352 (3) Hillenbrand, R.; Taubner, T.; Keilmann, F. *Nature* **2002**, *418*,
353 159–162.
- 354 (4) Brar, V. W.; Jang, M. S.; Sherrott, M.; Kim, S.; Lopez, J. J.; Kim,
355 L. B.; Choi, M.; Atwater, H. *Nano Lett.* **2014**, *14*, 3876–3880.
- 356 (5) Schlather, A. E.; Large, N.; Urban, A. S.; Nordlander, P.; Halas,
357 N. J. *Nano Lett.* **2013**, *13*, 3281–3286.
- 358 (6) Hale, G. D.; Jackson, J. B.; Shmakova, O. E.; Lee, T. R.; Halas, N.
359 J. *Appl. Phys. Lett.* **2001**, *78*, 1502–1504.
- 360 (7) Meinzer, N.; Ruther, M.; Linden, S.; Soukoulis, C. M.; Khitrova,
361 G.; Hendrickson, J.; Olitzky, J. D.; Gibbs, H. M.; Wegener, M. *Opt.*
362 *Express* **2010**, *18*, 24140–24151.
- 363 (8) Atwater, H. A.; Polman, A. *Nat. Mater.* **2010**, *9*, 205–213.
- 364 (9) Spinelli, P.; Ferry, V. E.; van de Groep, J.; van Lare, M.;
365 Verschuuren, M. A.; Schropp, R. E. I.; Atwater, H. A.; Polman, A. J.
366 *Opt.* **2012**, *14*, 024002.
- 367 (10) Okamoto, K.; Niki, I.; Shvartser, A.; Narukawa, Y.; Mukai, T.;
368 Scherer, A. *Nat. Mater.* **2004**, *3*, 601–605.
- 369 (11) Fofang, N. T.; Park, T.-H.; Neumann, O.; Mirin, N. A.;
370 Nordlander, P.; Halas, N. J. *Nano Lett.* **2008**, *8*, 3481–3487.
- 371 (12) Saxena, K.; Jain, V. K.; Mehta, D. S. *Opt. Mater.* **2009**, *32*, 221–
372 233.
- 373 (13) Stratakis, E.; Kymakis, E. *Mater. Today* **2013**, *16*, 133–146.
- 374 (14) Esfandyarpour, M.; Garnett, E. C.; Cui, Y.; McGehee, M. D.;
375 Brongersma, M. L. *Nat. Nanotechnol.* **2014**, *9*, 542–547.
- 376 (15) Gan, Q.; Bartoli, F. J.; Kafafi, Z. H. *Adv. Mater.* **2013**, *25*, 2385–
377 2396.
- 378 (16) Lidzey, D. G.; Bradley, D. D. C.; Skolnick, M. S.; Virgili, T.;
379 Walker, S.; Whittaker, D. M. *Nature* **1998**, *395*, 53–55.
- 380 (17) Wu, J.-L.; Chen, F.-C.; Hsiao, Y.-S.; Chien, F.-C.; Chen, P.; Kuo,
381 C.-H.; Huang, M. H.; Hsu, C.-S. *ACS Nano* **2011**, *5*, 959–967.
- 382 (18) Rainò, G.; Stöferle, T.; Park, C.; Kim, H.-C.; Topuria, T.; Rice,
383 P. M.; Chin, I.-J.; Miller, R. D.; Mahrt, R. F. *ACS Nano* **2011**, *5*, 3536–
384 3541.
- 385 (19) Heeger, A. J.; Kivelson, S.; Schrieffer, J. R.; Su, W. P. *Rev. Mod.*
386 *Phys.* **1988**, *60*, 781–850.
- 387 (20) Sirringhaus, H.; Brown, P. J.; Friend, R. H.; Nielsen, M. M.;
388 Bechgaard, K.; Langeveld-Voss, B. M. W.; Spiering, A. J. H.; Janssen, R.
389 A. J.; Meijer, E. W.; Herwig, P.; de Leeuw, D. M. *Nature* **1999**, *401*,
390 685–688.
- 391 (21) Alvarado, S. F.; Seidler, P. F.; Lidzey, D. G.; Bradley, D. D. C.
392 *Phys. Rev. Lett.* **1998**, *81*, 1082–1085.
- 393 (22) Brown, P. J.; Thomas, D. S.; Köhler, A.; Wilson, J. S.; Kim, J.-S.;
394 Ramsdale, C. M.; Sirringhaus, H.; Friend, R. H. *Phys. Rev. B: Condens.*
395 *Matter Mater. Phys.* **2003**, *67*, 064203.
- 396 (23) Jiang, X. M.; Osterbacka, R.; Korovyanko, O.; An, C. P.;
397 Horovitz, B.; Janssen, R. A. J.; Vardeny, Z. V. *Adv. Funct. Mater.* **2002**,
398 *12*, 587–597.
- 399 (24) Horovitz, B. *Solid State Commun.* **1982**, *41*, 729–734.
- 400 (25) Soci, C.; Moses, D.; Xu, Q.-H.; Heeger, A. J. *Phys. Rev. B:*
401 *Condens. Matter Mater. Phys.* **2005**, *72*, 245204.
- 402 (26) Deschler, F.; De Sio, A.; von Hauff, E.; Kutka, P.; Sauermann,
403 T.; Egelhaaf, H.-J.; Hauch, J.; Da Como, E. *Adv. Funct. Mater.* **2012**, *22*,
404 1461–1469.
- 405 (27) Österbacka, R.; An, C. P.; Jiang, X. M.; Vardeny, Z. V. *Science*
406 **2000**, *287*, 839–842.
- 407 (28) Cataldo, S.; Zhao, J.; Neubrech, F.; Frank, B.; Zhang, C.; Braun,
408 P. V.; Giessen, H. *ACS Nano* **2012**, *6*, 979–985.
- 409 (29) Zhao, J.; Frank, B.; Neubrech, F.; Zhang, C.; Braun, P. V.;
410 Giessen, H. *Beilstein J. Nanotechnol.* **2014**, *5*, 577–586.
- (30) Meinzer, N.; König, M.; Ruther, M.; Linden, S.; Khitrova, G.;
411 Gibbs, H. M.; Busch, K.; Wegener, M. *Appl. Phys. Lett.* **2011**, *99*, 412
111104.
- (31) Zuloaga, J.; Nordlander, P. *Nano Lett.* **2011**, *11*, 1280–1283. 414
- (32) Alonso-González, P.; Albella, P.; Neubrech, F.; Huck, C.; Chen, 415
J.; Golmar, F.; Casanova, F.; Hueso, L. E.; Pucci, A.; Aizpurua, J.;
416 Hillenbrand, R. *Phys. Rev. Lett.* **2013**, *110*, 203902. 417
- (33) Salvador, M.; MacLeod, B. A.; Hess, A.; Kulkarni, A. P.; 418
Munehika, K.; Chen, J. I. L.; Ginger, D. S. *ACS Nano* **2012**, *6*, 419
10024–10032. 420
- (34) Handloser, M.; Dunbar, R. B.; Wisnet, A.; Altpeter, P.; Scheu, 421
C.; Schmidt-Mende, L.; Hartschuh, A. *Nanotechnology* **2012**, *23*, 422
305402. 423
- (35) Soos, Z. G.; Hayden, G. W.; Girlando, A.; Painelli, A. *J. Chem.* 424
Phys. **1994**, *100*, 7144–7152. 425
- (36) Del Zoppo, M.; Castiglioni, C.; Zuliani, P.; Zerbi, G. In 426
Handbook of Conducting Polymers; Skotheim, T. A.; Elsenbaumer, R. L.,
427 Reynolds, J. R., Eds.; Marcel Dekker: New York, 1998. 428
- (37) Kim, Y. H.; Spiegel, D.; Hotta, S.; Heeger, A. J. *Phys. Rev. B:* 429
Condens. Matter Mater. Phys. **1988**, *38*, 5490–5495. 430
- (38) Diesinger, H.; Chan, E. A.; Yin, J.; Soci, C. In *Handbook of* 431
Organic Materials for Optical and (Opto)Electronic Devices: Properties
432 *and Applications*; Ostroverkhova, O., Ed.; Woodhead Publishing Ltd: 433
Cambridge, 2013. 434
- (39) Österbacka, R.; Jiang, X. M.; An, C. P.; Horovitz, B.; Vardeny, Z. 435
Phys. Rev. Lett. **2002**, *88*, 226401. 436
- (40) Di Nuzzo, D.; Fontanesi, C.; Jones, R.; Allard, S.; Dumsch, I.; 437
Scherf, U.; von Hauff, E.; Schumacher, S.; Da Como, E. *Nat. Commun.* 438
2015, *6*, 6460. 439
- (41) Silva, C.; Dhoot, A. S.; Russell, D. M.; Stevens, M. A.; Arias, A. 440
C.; MacKenzie, J. D.; Greenham, N. C.; Friend, R. H.; Setayesh, S.;
441 Müllen, K. *Phys. Rev. B: Condens. Matter Mater. Phys.* **2001**, *64*, 125211. 442
- (42) Moses, D.; Soci, C.; Chi, X.; Ramirez, A. P. *Phys. Rev. Lett.* **2006**, 443
97, 067401. 444
- (43) Arkhipov, V. I.; Bäessler, H.; Deussen, M.; Göbel, E. O.; Lemmer, 445
U.; Mahrt, R. F. *J. Non-Cryst. Solids* **1996**, *198–200* (Part 2), 661–664. 446
- (44) Guo, J.; Ohkita, H.; Bente, H.; Ito, S. *J. Am. Chem. Soc.* **2009**, 447
131, 16869–16880. 448
- (45) Miranda, P. B.; Moses, D.; Heeger, A. J. *Phys. Rev. B: Condens.* 449
Matter Mater. Phys. **2004**, *70*, 085212. 450
- (46) Sheng, C. X.; Tong, M.; Singh, S.; Vardeny, Z. V. *Phys. Rev. B:* 451
Condens. Matter Mater. Phys. **2007**, *75*, 085206. 452
- (47) Tautz, R.; Da Como, E.; Wiebeler, C.; Soavi, G.; Dumsch, I.; 453
Fröhlich, N.; Grancini, G.; Allard, S.; Scherf, U.; Cerullo, G.; 454
Schumacher, S.; Feldmann, J. *J. Am. Chem. Soc.* **2013**, *135*, 4282–4290. 455
- (48) Gadermaier, C.; Cerullo, G.; Sansone, G.; Leising, G.; Scherf, 456
U.; Lanzani, G. *Phys. Rev. Lett.* **2002**, *89*, 117402. 457
- (49) Bakulin, A. A.; Rao, A.; Pavelyev, V. G.; van Loosdrecht, P. H. 458
M.; Pshenichnikov, M. S.; Niedzialek, D.; Cornil, J.; Beljonne, D.;
459 Friend, R. H. *Science* **2012**, *335*, 1340–1344. 460
- (50) Grancini, G.; Maiuri, M.; Fazzi, D.; Petrozza, A.; Egelhaaf, H. J.; 461
Brida, D.; Cerullo, G.; Lanzani, G. *Nat. Mater.* **2012**, *12*, 29–33. 462
- (51) Mihailović, D.; Foster, C. M.; Voss, K.; Heeger, A. J. *Phys. Rev.* 463
B: Condens. Matter Mater. Phys. **1990**, *42*, 7989–7993. 464
- (52) Shelton, D. J.; Brener, I.; Ginn, J. C.; Sinclair, M. B.; Peters, D. 465
W.; Coffey, K. R.; Boreman, G. D. *Nano Lett.* **2011**, *11*, 2104–2108. 466